DEMONSTRATION OF SEPARATION CONTROL USING GLOW-DISCHARGE PLASMA ACTUATORS

Lennart S. Hultgren* **and David E. Ashpis†**

National Aeronautics and Space Administration

Glenn Research Center at Lewis Field

Cleveland, Ohio 44135, USA

Email: Lennart.S.Hultgren@grc.nasa.gov David.E.Ashpis@grc.nasa.gov

Abstract

Active flow control of boundary-layer separation using glow-discharge plasma actuators is studied experimentally. Separation is induced on a flat plate installed in a closed-circuit wind tunnel by a shaped insert on the opposite wall. The flow conditions represent flow over the suction surface of a modern low-pressure-turbine airfoil. The Reynolds number, based on wetted plate length and nominal exit velocity, is varied from 50,000 to 300,000, covering cruise to takeoff conditions. Low (0.2%) and high (2.5%) free-stream turbulence intensities are set using passive grids. A spanwise-oriented phased-plasma-array actuator, fabricated on a printed circuit board, is surface-flush-mounted upstream of the separation point and can provide forcing in a wide frequency range. Static surface pressure measurements and hot-wire anemometry of the base and controlled flows are performed and indicate that the glow-discharge plasma actuator is an effective device for separation control.

1 Introduction

Modern low-pressure turbines, in general, utilize highly loaded airfoils in an effort to improve efficiency and to lower the number of airfoils needed. Typically, the airfoil boundary layers are turbulent and fully attached at takeoff conditions, whereas a substantial fraction of the boundary layers on the airfoils may be transitional at cruise conditions due to the change of density with altitude [1]. The strong adverse pressure gradients on the suction side of these airfoils

*Associate Fellow AIAA

†Senior Member AIAA

can lead to boundary-layer separation at the latter (low Reynolds number) conditions. Large separation bubbles, particularly those which fail to reattach, cause a significant degradation of engine efficiency [1–3]. A component efficiency drop of the order 2% may occur between takeoff and cruise conditions for large commercial transport engines and could be as large as 7% for smaller engines at higher altitude. An efficient means of of separation elimination/reduction is, therefore, crucial to improved turbine design.

The large change in the Reynolds number from takeoff to cruise leads to a distinct change in the airfoil flow physics. Consequently, further airfoil shape optimization, with the constraint of high power at takeoff, cannot be expected to eliminate separation at cruise. Future more aggressive high-lift designs may also further aggravate the situation. Clearly, a separation control strategy needs to be developed for cruise conditions with minimum impact/penalty at takeoff.

A complicating factor, but also a potential advantage in the quest for an efficient strategy, is the intricate interplay between separation and transition for the situation at hand. Transition may begin before or after separation, depending on the Reynolds number and other flow conditions. If the transition occurs early in the boundary layer then separation may be reduced or completely eliminated. Transition in the shear layer of a separation bubble can lead to rapid reattachment. This suggests using control mechanisms to trigger and enhance early transition.

Further complicating the problem are the high free-stream turbulence levels in a real engine environment, the strong pressure gradients along the airfoils, the curvature of the airfoils, and the unsteadiness associated with wake passing from upstream stages. Because of the complicated flow situation, transition in these devices can take many paths that can coexist, vary in importance, and possibly also interact, at different locations and instances in time. Volino [4] gives a comprehensive discussion of several recent studies on transition and separation under low-pressure-turbine conditions, among them one in the present facility [5].

Gad-el-Hak [6] provides a review of various techniques for flow control in general and Volino [7] discusses recent studies on separation control under low-pressure-turbine conditions. The latter includes techniques utilizing passive [8–10] as well as active [7, 11–18] devices. As pointed out by Volino [7], passive devices optimized for separation control at low Reynolds numbers tend to increase losses at high Reynolds numbers. Active devices have the attractive feature that they can be utilized only in operational regimes where they are needed and when turned off would not affect the flow. The focus in the present paper is active separation control using glow discharge plasma actuators.

As in [5], the boundary layer on a flat plate is subject to a streamwise pressure gradient corresponding to that on the suction side of the 'Pak-B' airfoil. Reynolds numbers from 50,000 to 300,0000 are considered, spanning the range from cruise to takeoff conditions. Cases with high (nominal 7%) and low (0.2%) inlet free-stream turbulence are documented. As will be seen later, these inlet TI levels in the present study correspond to about 0.2% and 2.5% in the test section when normalized with the exit velocity. Free-stream turbulence levels in low-pressure turbines could be

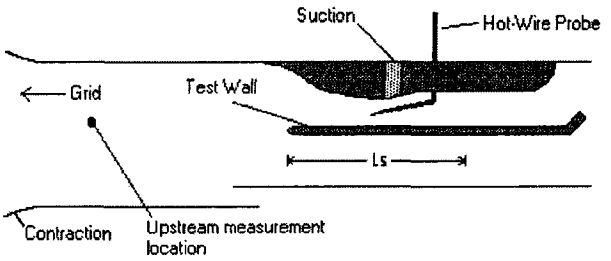

Figure 1: Schematic of the test section, side view, approximately to scale, L_s=208 mm (wetted length, streamwise length is 206 mm)

as low as about 3% ([19]) on the suction side of the airfoils. The present high TI case, therefore, represents a realistic value. A spanwise-oriented phased-plasma-array [20] actuator, fabricated on a printed circuit board, is surface-flush-mounted upstream of the separation point and can provide forcing in a wide frequency range. Static surface pressure measurements and single-wire constant-temperature anemometry of the base and controlled flows are performed.

2 Experimental Facility

All experiments were conducted in a low-speed, recirculating wind tunnel. The wind tunnel was used in earlier studies, such as [5, 21, 22]. A blower capable of 4.72 m^3s^{-1} (10,000 CFM), with an 18.6 kW (25 HP) motor and variable speed controller, supplies air to a rectangular channel of cross section 0.635 m $\times$ 0.686 m. The channel contains a series of screens and flow straighteners. Turbulence generating grids may be placed at the exit of the channel. As in [5], a coarse grid with 40% blockage, constructed with 50 mm wide, 13 mm thick (in the streamwise direction) vertical and horizontal bars, was used for the high TI case. Grid spacing is 178 mm. For the low TI case, no grid was used. Just downstream (29 mm) of the grid location is an 0.914 m long, two-dimensional contraction, which reduces the flow area to 0.178 m $\times$ 0.686 m. The long dimension is horizontal, the shorter is vertical. Following the contraction is an 0.245 m long straight section at the end of which is an upstream facing double bleed-scoop, located at the bottom of the channel, that further reduces the vertical dimension to 0.152 m. Following this is a rectangular channel which serves as the test section. A side view schematic of the test section is shown in Figure 1.

A 12.7 mm thick horizontal Plexiglas plate with a 4:1 elliptical leading edge is mounted with its top surface at the vertical center of the channel, spanning the 0.686 m width, and with its leading edge 54 mm downstream of the beginning of the test section. The leading edge is, hence, 0.299 m downstream of the end of the contraction and 1.242 m downstream of the grid location. The upper surface of the plate is the test wall for the experiments. The same two-dimensional contoured shape as in [5] is attached to the wall opposite the test wall to produce the desired 'Pak-B' pressure gradient along the test wall.

In a cascade experiment, favorable pressure gradients prevent separation on the pressure side of the airfoils. In

the present situation, however, suction is needed to insure that the flow remains attached on the contoured wall and separates only on the test wall. Suction was applied through holes along a 30 mm $\times$ 0.686 m strip in the contoured wall, just downstream of the throat (position of maximum free-stream velocity). A blower with an 0.75 kW (1 HP) electric motor and variable speed controller was used to produce the suction. The blower speed was adjusted linearly with the Reynolds number considered, to prevent separation and to produce the desired minimum pressure along the test plate at the throat. In addition, the contoured wall was covered by sandpaper upstream as well as a short distance downstream of the suction slot to promote a turbulent boundary layer on that surface via tripping. This is identical to the arrangement used in Volino and Hultgren [5].

Downstream of the test section, the flow entered a diffuser, then was routed through filters and a heat exchanger (cooler) before returning to the blower. The latter, of course, is needed to keep the wind-tunnel operating temperature from drifting.

2.1 Actuator

A phased-plasma-array [20] actuator, is surface-flush-mounted just upstream of the separation point. The insert is of 89 mm streamwise length and 119 mm spanwise extent. The actuator was fabricated in-house, using printed-circuit-board technology, and has seven spanwise-oriented electrode pairs with an effective spanwise length of 77.5 mm. The design is shown in Fig. 2 and is an improvement of early designs [23] by a research group at University of Notre Dame. The

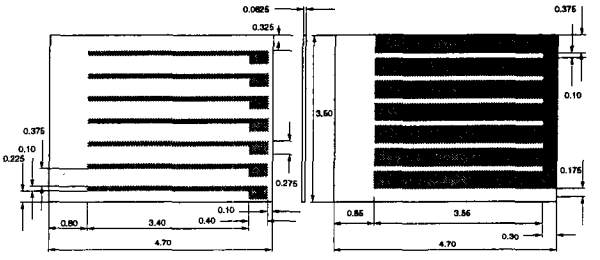

Figure 2: Actuator design, top view and bottom view; corners at figure center are the same; flow direction from bottom to top; dimensions in inches, 25.4 mm

streamwise electrode offset leads to a glow discharge plasma only on the downstream side of the top electrodes. This asymmetric arrangement has been shown to be advantageous [23] in that it leads to an effective forcing of the fluid. The computer controlled actuator driver circuits are illustrated in Fig. 3. They consists of a National Instrument eight channel (only five used at present) digital-to-analog output PCI card (PCI-6713) for the top electrodes and a GPIB controlled Stanford Research Systems synthesized function generator (DS345) for the common bottom electrodes. The analog outputs are each fed into 1:10 operational amplifier circuits and then into 1:120 transformers producing voltages in the kV range at the actuator. In the present arrangement, the top electrodes are, in turn, fed a sequence

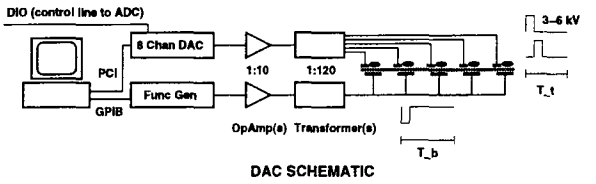

Figure 3: Actuator driver-circuit schematic

Table 1: Station locations in Volino and Hultgren [5].

Station	1	2	3	4	5	6	7
s/L_s	0.28	0.33	0.39	0.45	0.51	0.57	0.63
Station	8	9	10	11	12	13	14
s/L_s	0.69	0.75	0.81	0.88	0.94	1.00	1.06

of (positive) pulses with a repeat rate $1/T_t = 4$ kHz, where T_t is the period. The common bottom electrodes are fed a pulse train of opposite polarity (negative) with a slightly different period T_b. The frequency difference gives rise to a beat frequency of the glow-discharge plasma and this is what leads to an unsteady forcing of the flow. This arrangement can provide forcing in a wide frequency range. See Roth [24] for more details about plasma in general and for glow-discharge plasma actuator applications for flow control see Refs. [20, 23, 25].

2.2 Instrumentation

The flat plate has 45 static pressure taps and a pitot tube was used to obtain the exit velocity of the simulated blade. The pressure measurement system consists of a Scanivalve Corporation 48 port J-type multiplexer connected selectively to two Druck (LPM 9381) differential pressure transducers of ± 0.1kPa and ± 1kPa ranges, respectively. This allows for accurate pressure measurements for the full Reynolds number range of the present study. A GPIB controlled digitizer was used to acquire the output voltages from the pressure transducers and its digital input-output lines were used to control the pressure multiplexer.

Streamwise velocity was measured using a single sensor hot-wire probe with a 5 μm diameter platinum wire. The probe was inserted through a slot in the spanwise center of the top wall of the test section, and could be traversed in the streamwise direction and normal to the test wall. Traversing was accomplished using stepper motors controlled by the same computer used for data acquisition. Velocity profiles were acquired at the streamwise stations 9 through 13 listed in Table 1. Each profile consisted of 41 points spaced normal to the wall, with finer spacing closer to the wall. Voltage data were acquired from the constant-temperature anemometer using a 16 bit digitizer, controlled through an IEEE 488 interface bus (GPIB) with a computer. At each measurement location, 53 s long time records were acquired consisting of just over 1 million ($1,048,576 = 2^{20}$) data points collected at a 20 kHz sampling rate using an anti-aliasing 8.3

kHz low-pass filter before sampling. Uncertainty in mean and fluctuating velocities is 5%, which is primarily due to bias error resulting from calibration uncertainty.

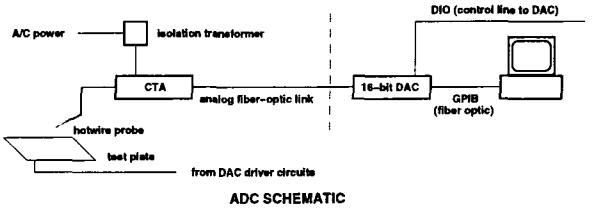

Figure 4: Fiber-optic link isolation

An important concern when working with glow-discharge plasma is how to protect sensitive electronic components from damage due to potential buildup of high electrostatic charges. Fig 4 indicates how the hot-wire constant temperature anemometry is isolated from the analog-to-digital converters using a analog fiber-optic link (AA Labs AFL-500, $\pm$10V DC-20kHz) and an isolation transformer for the CTA power supply.

3 Results

Experimental data were acquired with freestream TI of 0.2% and 2.5%. The nature of the turbulence at these two levels is briefly discussed in Volino and Hultgren [5] where cross-wire measurements were also taken at the exit of the contraction, see Fig 1. In the low TI case, most of the intensity is due to low frequency streamwise unsteadiness, as opposed to turbulent eddies. Downstream in the test section, the TI remains essentially unchanged at about 0.2%, despite the strong acceleration over the leading section of the test wall. In the high TI case at the contraction exit, the turbulence is non-isentropic, since the grid is located upstream of the contraction, and at about 7% intensity. The integral scales are comparable to the width of the bars of the grid, and are representative of the large eddies in the free-stream. Downstream, over the test wall, the TI is reduced to about 2.5% due in part to decay of the free-stream turbulence, but mainly due to the increase in mean free-stream velocity as the flow is accelerated. The ratio of the free-stream velocity at the exit of the contraction to the velocity in the throat is 0.45. Qiu and Simon [26] had the same ratio of inlet to throat velocity in their cascade experiment.

Streamwise pressure profiles for the Reynolds numbers of 50,000, 100,000, 200,000 and 300,000, are shown in Figure 5 along with the expected profile for the suction side of the 'Pak-B' airfoil. The pressure coefficients, C_p, were computed from static pressure measurements using the exit velocity obtained from the pitot tube. The streamwise distance is normalized on the nominal suction surface length (207.55 mm). The Reynolds number is based on the nominal suction surface length and the exit velocity. The actual plate is 356 mm long and there are several pressure taps downstream of the point which represents the trailing edge of the airfoil. The pressure profiles upstream of the throat are in good agreement with the 'Pak-B' profile for all cases. Downstream, the agreement is good for the high

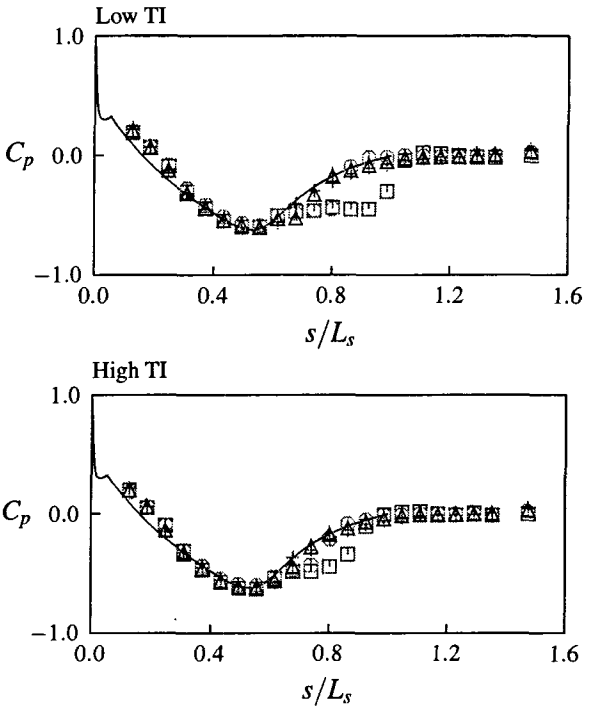

Figure 5: C_p profiles: (a) Low TI, (b) High TI; Re = 50,0000 (square), 100,000 (circle), 200,000 (triangle), 300,000 (plus)

Re, high TI cases. At the lower Reynolds numbers, the C_p values indicate separation. At low TI and Re=50,000, the boundary layer may not be fully reattached at the end of the modeled airfoil.

The following two subsections will describe results from pressure and hot-wire measurements, respectively, showing the effects of using the glow-discharge plasma actuator for active separation control. In all cases described herein, the five most downstream electrode pairs were used in such a way that the plasma repeatedly moves from electrode pair to electrode pair in the downstream direction. The base frequency for the plasma generation was 4 kHz and the delta frequency (or detuning) between the pulse trains for the top and bottom electrodes, which leads to the sequential plasma pulsing, was varied in order to study the frequency dependency of the control mechanism. The gain in the signal generating circuits was set so that an active electrode pair would have a voltage difference of 3.84 kV.

3.1 Pressure Measurements

Figure 6 shows the impact on the C_p profile by using the actuator at a typical delta frequency for Re = 50,0000. The top and bottom panels are for the low and high TI cases, respectively. The negative delta frequency, $\Delta f = -48.992$ Hz, indicates that the pulse train on the bottom electrodes is at a lower frequency than that for the upper ones and, consequently, that the plasma forms repeatedly and sequentially in the downstream direction for the last five electrode

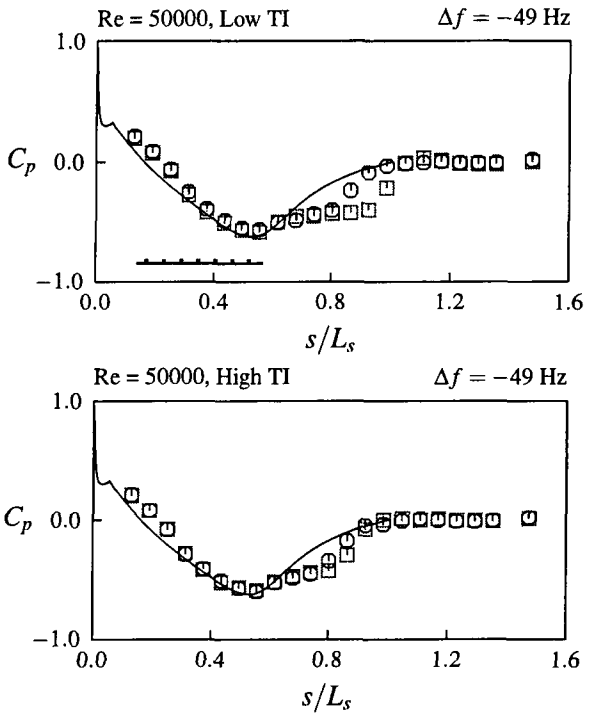

Figure 6: C_p profiles: (a) Low TI, (b) High TI; actuator off (square) and on (circle)

pairs. The horizontal line in (a) indicates the location of the actuator (from 0.14 to 0.57 in nondimensional coordinates) and the dashes above this line shows the location of the upper electrodes. The glow-discharge plasma forms at the downstream edge of these. As can be seen in the low TI case, the separated region is reduced and the theoretical profile is recovered before the end of the modeled airfoil. In the high TI case, the separation is already much less drastic than in the low TI case, but even here an improvement can be seen with the actuator turned on.

For the low TI case at Re = 50,000, the actuator was found to be effective in reducing the separation for forcing frequencies, $f_b = |\Delta f|$, between roughly 30 to 150 Hz with results very similar to that shown in Fig. 6(a). Qualitatively speaking, the effectiveness is rather flat in this region and then gradually drops off. The C_p distribution was affected, but much less so, also for frequencies outside of this range like, say, 10 Hz and 200Hz and above. The effective range expressed in terms of a nondimensional frequency parameter F_+, f_b scaled with the suction surface distance between the pressure minimum and the trailing edge of the modeled airfoil and the nominal exit velocity, is estimated to be about 0.6–3. The sign of the delta frequency turned out not to change the effectiveness of the actuator. That is, positive values of Δf where the plasma forms sequentially in the upstream direction, worked as well as negative ones. This leads to the hypothesis, which will be tested in future work, that only the plasma at the last electrode pair adds the most significant unsteady forcing to the flow because of its proximity to the separation point and the strong favorable pressure gradient over nearly all of the actuator.

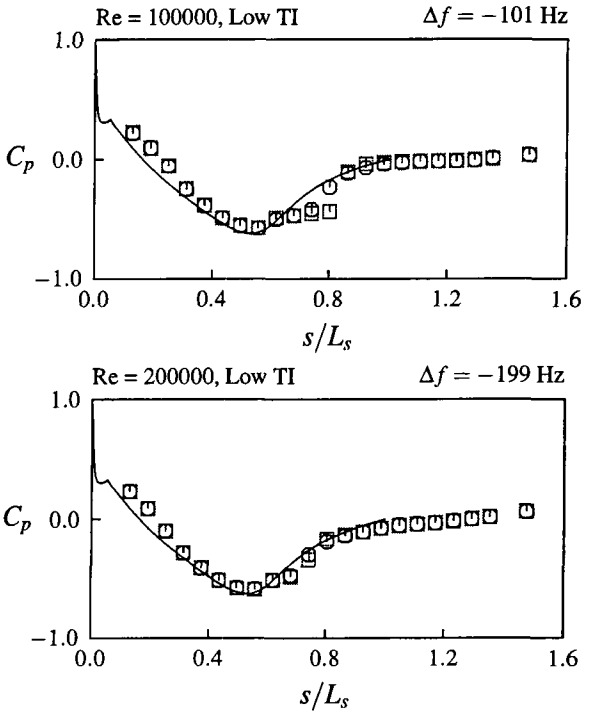

Figure 7: C_p profiles: (a) Low TI, (b) High TI; actuator off (square) and on (circle)

Figure 7 shows the effect of operating the actuator for low TI and Re = 100,0000 (top panel) and 200,000 (bottom panel) at difference frequencies of -101.36 Hz and -199.16 Hz, respectively, i.e., essentially at the same nondimensional frequency F_+ as the cases in Fig. 6. It can be seen that with the actuator inactive and Re = 100,000, there is a clear indication in the C_p distribution of a separation bubble with a length about half as long as in the corresponding case at Re = 50,000. The effect of the actuator is also here to reduce the separated region. In the Re = 200,000 case, the unforced flow is nearly fully attached and the effect of the actuator is minimal.

The results indicate that the present, spanwise oriented, actuator works by promoting transition in the shear layer of the separation bubble which then leads to earlier reattachment. This conclusion will be further supported by the hot-wire measurements described in the next subsection.

3.2 Hot-Wire Measurements

The mean streamwise velocity profiles and streamwise fluctuating velocity profiles are shown for the streamwise stations 9–13 of the low TI, Re=50,000 case in Fig. 8. The velocity profiles are normalized using the nominal free-stream exit velocity, obtained from the exit pitot tube measurements, which would correspond to the free-stream velocity at the last station if the boundary layer is attached there. The surface normal coordinate is normalized using the wetted surface length of the modeled airfoil and scaled by the square root of the Reynolds number. This represents

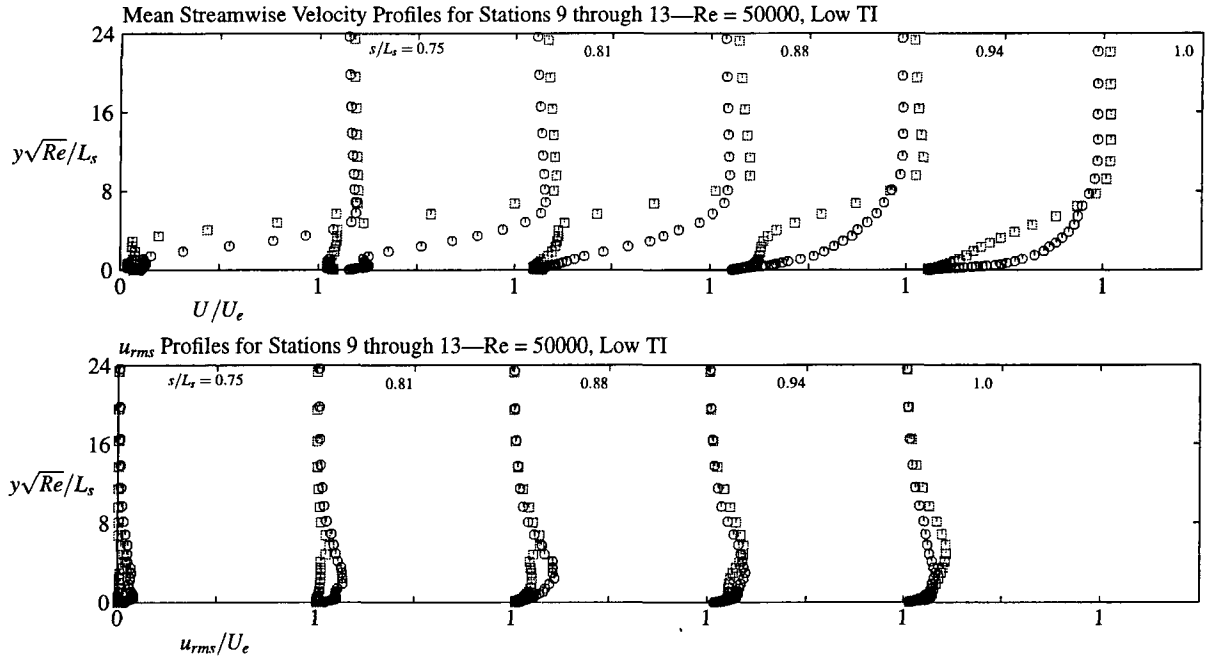

Figure 8: Profiles for Low TI, Re=50,000 case: (a) Mean velocity, (b) u_{rms}; actuator off (square) and on (circle)

a natural boundary-layer type normalization and scaling. The very near-wall behavior of the mean flow profiles in this figure and a later one is to be considered preliminary since the issue of near-wall correction of the hot-wire measurements has not yet been addressed here.

In the case of the actuator being turned off, the top panel of Fig. 8 (squares) shows that the boundary layer is clearly separated at stations 9 and 10 and that the separation bubble is growing. At stations 11 and 12, the low, but non-zero velocities near the wall indicate that the boundary layer is beginning to reattach, although it may be intermittently separated and attached at these locations. At station 13, representing the end of the airfoil in question, the mean velocity profile indicates that the boundary layer is reattached at this Re and TI. The corresponding fluctuating velocity profiles (squares) in the bottom panel of this figure show very low turbulence at stations 9 and 10, with a slight increase in u_{rms} just above the separation bubble seen in the mean profile. The u_{rms} fluctuations continue to grow in the shear layer over the separation bubble at Stations 9 through 12. The u_{rms} level is still very low inside the bubble at stations 9 and 10, indicating that the flow is largely stagnant in this region. This is expected based on the near-zero mean velocity in the separation bubble. Since the hot-wire can not distinguish flow direction, a reversing or turbulent flow in the separation bubble would have resulted in false positive mean velocity if the magnitude of the fluctuations were significant. At station 11, significant u_{rms} fluctuations also begin to appear near the wall. This indicates that the boundary layer is starting to reattach. The fluctuations are also extending farther from the wall toward the free-stream. By the last station, the u_{rms} profile shows significant fluctuations starting near the wall and well out into the freestream,

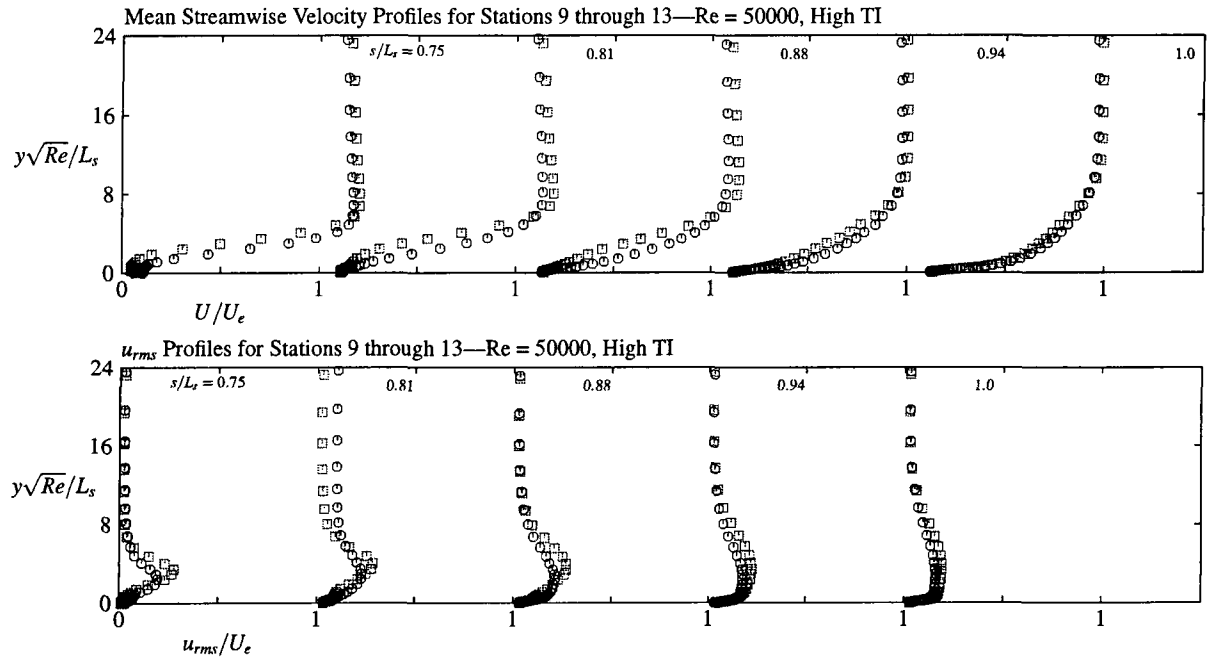

Figure 9: Profiles for High TI, Re=50,000 case: (a) Mean velocity, (b) u_{rms}; actuator off (square) and on (circle)

indicating that transition in the shear layer over the separation bubble has reattached the flow.

In the case of the actuator being used, with the same delta frequency (-48.992 Hz) as before, Fig. 8 (circles) shows that the boundary layer now is starting to reattach already at station 9 and that the flow is reattached by station 11. The separation bubble is thus much shorter as well as thinner. Consistent with this picture, significant unsteady fluctuations now also occurs near the wall and well out into the freestream already at station 11. The broadening of the peak in the u_{rms} distribution towards the wall from stations 11 through 13 indicates that an attached turbulent or transitional boundary layer is developing.

The velocity profiles for the high TI, Re=50,000 case are shown in Fig. 9. In the case of the actuator not operating (squares), the boundary layer is separated, at stations 9 and 10, but the thickness of the separation bubble is only about half that of the corresponding low TI case at station 9. At station 11, the boundary layer has just reattached, and the profile shape recovers to that of an attached turbulent boundary layer through stations 12 and 13. In the corresponding low TI case, reattachment did not occur until station 13. At station 9, the u_{rms} profile show a pronounced peak at the location of the maximum shear of the mean profile, i.e. in the shear layer over the separation bubble. This peak spreads towards the wall as the flow reattaches. The absence of a pronounced near-wall peak at station 13 indicates that the turbulent boundary-layer flow at this location is still recovering from the upstream separation.

In the case of the actuator being turned on (circles), Fig. 9 shows that the reattachment process is somewhat accelerated compared to when it is not. However, the profiles at the last station are quite similar. This suggests that the

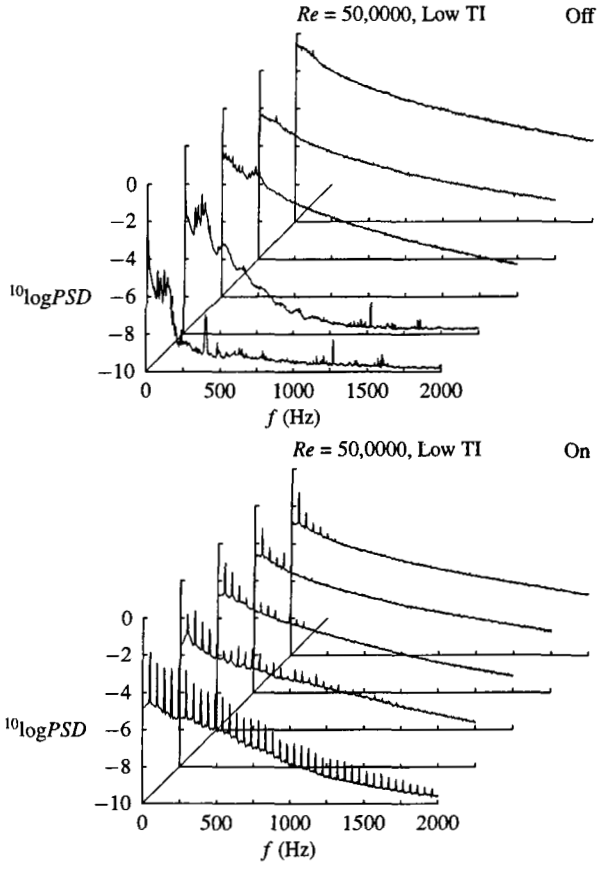

Figure 10: u' power spectrum densities at locations of maximum u_{rms} at stations 9–13 for Low TI, Re=50,000 case: (a) actuator off, (b) actuator on

actuator is most effective in modifying the flow in the shear layer above the separation bubble and that it has limited (if any) further effect once the flow has reattached.

Figures 10 and 11 show the evolution of the u' power spectral densities at the locations of maximum u_{rms} in the flow for successive downstream station (9–13) in the low and high TI cases, respectively. The top panel in Fig. 10 is for Re = 50,000, low TI, and the actuator turned off. The front curve shows that the fluctuations mainly occur at very low frequencies and in a band centered about 125 Hz, the latter due to shear layer instability, at station 9. At higher frequencies the magnitude is still low, indicating that the flow is not yet turbulent. At station 10, the shear layer instability has increased in magnitude, significant higher harmonics have been generated, and the shear layer can be interpreted to be in its later stages of transition. Between stations 10 and 11 there is a sudden jump to higher levels at higher frequencies, indicating a transition to turbulence. Thus, the shear layer is turbulent at stations 11 and 12. The curve for the last station in combination with the corresponding results in Fig. 8 indicate reattached turbulent flow.

The bottom panel in Fig. 10 corresponds to the case in the top panel but with the actuator turned on. Distinct peaks

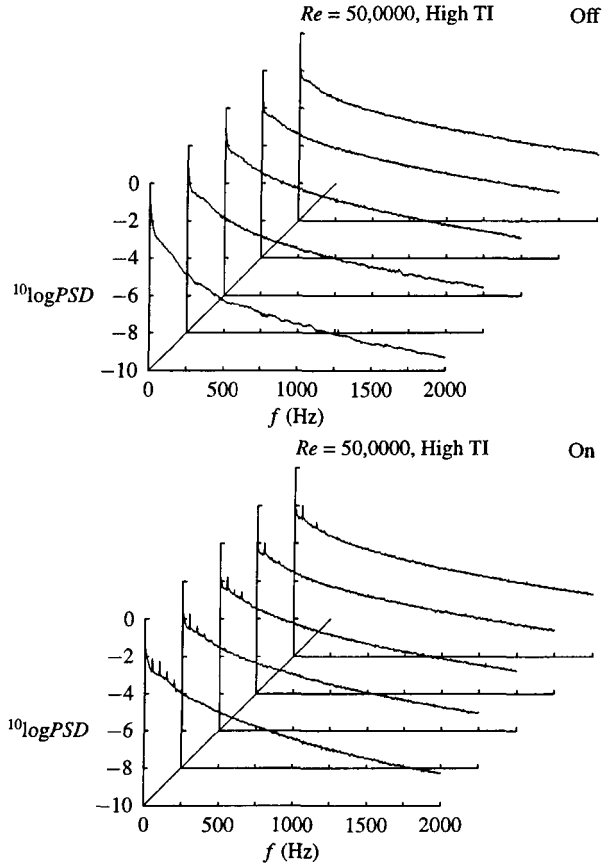

Figure 11: u' power spectrum densities at locations of maximum u_{rms} at stations 9–13 for High TI, Re=50,000 case: (a) actuator off, (b) actuator on

at the unsteady forcing frequency and its harmonics can be seen in the curve for station 9. The overall shape of the curve is also of a turbulent nature. This suggests that effect of the actuator is to have nearly, if not already, transitioned the shear layer flow to turbulence at this station. At station 10, the increased level at the higher frequencies indicates clearly that the shear layer now is turbulent. The effective range of forcing frequencies noted in the previous subsection can now be understood in terms of the frequency band for instability waves in the separated shear layer. The the later curves, in combination with the corresponding results in Fig. 8 indicate reattached turbulent flow at stations 11–13.

The top panel in Fig. 11 is for Re = 50,000, high TI, and the actuator turned off. Comparing to Fig. 10, there is considerably more fluctuation energy in the high TI case at the first station than in the low TI case. This energy is induced by the free-stream over all frequencies, with no frequency spikes, but with lower frequencies more successful in penetrating the upstream boundary layer. This penetration occurs already at the stations upstream of the ones presented here. Volino and Hultgren [5] documented the slow but steady growth of these low-frequency disturbances, induced by the free-stream fluctuations [27–29] and detectable as a near-wall peak in the u_{rms} distribution, through

the favorable pressure gradient region upstream of the boundary-layer separation location and their movement away from the wall and into the still laminar shear layer over the separation bubble. The later curves in the top panel of Fig. 11 show no amplification of select instabilities as in the top panel of Fig 10 but rather a rising energy level across the entire spectrum as transition proceeds. This indicates that transition occurs through a bypass mode, rather than the breakdown of the instability waves seen in the low TI case [5, 28]. Downstream of transition, the spectra for the low and high TI cases are essentially the same.

The bottom panel in Fig. 11 is for the case in the top pannel but with the actuator being used. The level at higher frequencies is increased at station 9 compared to the unforced case in the top panel indicating that using the actuator has accelerated the transition process. The curves at the last three stations are very similar for both cases in this figure indicating the limited further effect of the forcing once transition to turbulence has occurred.

4 Summary

Active flow control of boundary layer separation using a glow-discharge plasma actuator has been documented under Reynolds number and pressure gradient conditions typical of low-pressure turbine airfoils. The present spanwise-oriented phased-plasma-array actuator, located upstream of the separation point, has been found effective for separation control. The results suggest that the actuator works by promoting early transition in the shear layer above the separation bubble thus leading to rapid reattachment. The actuator is effective in a frequency band corresponding to the range of instability waves in the separated shear layer. It is particularly effective under low free-stream turbulence conditions where the boundary layer is laminar at separation. It also accelerates transition and subsequent reattachment under high freestream turbulence conditions, where the pre-transitional boundary layer separates at about the same location as in the low freestream turbulence case and the shear layer transition occurs through a bypass mode.

The authors wish to thank Prof. T. C. Corke for helpful advice and open discussions.

References

[1] Mayle, R.E., "The Role of Laminar-Turbulent Transition in Gas Turbine Engines," *J. Turbomachinery* **113**, 509-537 (1991).

[2] Hourmouziadis, J., "Aerodynamic Design of Low Pressure Turbines," AGARD Lecture Series 167, (1989).

[3] Sharma, O.P., Ni, R.H. and Tanrikut, S., "Unsteady Flow in Turbines," AGARD-LS-195, Paper No. 5, (1994).

[4] Volino, R. J., "Separated Flow Transition Under Simulated Low-Pressure Turbine Airfoil Conditions: Part 1—Mean Flow and Turbulence Statistics," *J. Turbomachinery* **124**, 645-655 (2002). Also ASME Paper 2002-GT-30236 (2002).

[5] Volino, R. J. and Hultgren, L. S., "Measurements in Separated and Transitional Boundary Layers Under Low-

Pressure Turbine Airfoil Conditions," *J. Turbomachinery* **123**, 189-197, (2001). Also ASME Paper 2000-GT-0260 (2000).

[6] Gad-el-Hak, M. *Flow Control, Passive, Active, and Reactive Flow Management*, Cambridge Univ. Press, Cambridge (2000).

[7] Volino, R. J., "Separation Control on Low-Pressure Turbine Airfoils Using Synthetic Vortex Generator Jets," ASME Paper 2003-GT-38729 (2003).

[8] Lake, J. P., King, P. I. and Rivir, R. B., "Low Reynolds Number Loss Reduction on Turbine Blades with Dimples and V-Grooves," AIAA Paper 2000-0738 (2000).

[9] Van Treuren, K. W., Simon, T., von Koller, M., Byerley, A. R., Baughn, J. W. and Rivir, R. B., "Measurements in a Turbine Cascade Flow Under Ultra Low Reynolds Number Conditions," *J. Turbomachinery* **124**, 100-106 (2002). Also ASME Paper 2001-GT-164 (2001).

[10] Volino, R. J., "Passive Flow Control on Low-Pressure Turbine Airfoils," ASME Paper 2003-GT-38728 (2003).

[11] Bons, J. P., Sondergard, R. and Rivir, R. B., "Turbine Separation Control Using Pulsed Vortex Generator Jets," *J. Turbomachinery* **123**, 198-206 (2001). Also ASME Paper 2000-GT-262 (2000).

[12] Bons, J. P., Sondergard, R. and Rivir, R. B., "The Fluid Dynamics of LPT Blade Separation Control Using Pulsed Jets," *J. Turbomachinery* **124**, 77-85 (2002). Also ASME Paper 2001-GT-190 (2001).

[13] Volino, R. J., "Separation Control Using Synthetic Vortex Generator Jets," *Bull. Amer. Phys. Soc.* **47**, No. 10, 82 (2002).

[14] Huang, J., Corke, T. C. and Thomas, F. O., "Separation Control over Low Pressure Turbine Blades," *Bull. Amer. Phys. Soc.* **47**, No. 10, 167 (2002).

[15] Hultgren, L. S. and Ashpis, D. E., "Glow Discharge Plasma Active Control of Separation Control at Low Pressure Turbine Conditions," *Bull. Amer. Phys. Soc.* **47**, No. 10, 167 (2002).

[16] Hultgren, L. S. and Ashpis, D. E., "Demonstartion of Separation Delay with Glow-Discharge Plasma Actuators," AIAA Paper 2003-1025 (2003).

[17] List, J., Byerley, A., McLaughlin, T. and Van Dyken, R., "Using Plasma Actuators Flaps to Control Laminar Separation on Turbine Blades in a Linear Cascade," AIAA Paper 2003-1026 (2003).

[18] Huang, J., Corke, T. C. and Thomas, F. O., "Plasma Actuators for Separation Control of Low Pressure Turbine Blades," AIAA Paper 2003-1027 (2003).

[19] Halstead, D.E., Walker, G.J., Wisler, D.C., Hodson, H.P., Okiishi, T.H. and Shin, H.-W., 1997, "Boundary Layer

Development in Axial Compressors and Turbines: Part 3 of 4 - LP Turbines," *J. Turbomachinery* **119**, 234-246 (1997).

[20] Corke, T. C. and Matlis, E., "Phased Plasma Arrays for Unsteady Flow Control," AIAA Paper 2000-2323 (2000).

[21] Sohn, K.H. and Reshotko, E., "Experimental Study of Boundary Layer Transition with Elevated Freestream Turbulence on a Heated Flat Plate," NASA CR 187068 (1991).

[22] Sohn, K.H., DeWitt, K.J. and Shyne, R.J., "Experimental Investigation of Boundary Layer Behavior in a Simulated Low Pressure Turbine," ASME paper 98-GT-034 (1998).

[23] Post, M. L., "Phased Plasma Actuators for Unsteady Flow Control," M.S. Thesis, University of Notre Dame (2001).

[24] Roth, J. R., *Industrial Plasma Engineering, Volume I—Principles*, Institute of Physics, Bristol (1995).

[25] Roth, J. R., Sherman, D. M. and Wilkinson, S. P., "Boundary Layer Flow Control with One Atmospheric Uniform Glow Discharge Surface Plasma," AIAA Paper 98-0328 (1998).

[26] Qiu, S. and Simon, T. W., "An Experimental Investigation of Transition as Applied to Low Pressure Turbine Suction Surface Flows," ASME paper 97-GT-455 (1997).

[27] Dryden, H. L., "Air flow in the boundary layer near a plate," NACA Report 562 (1936).

[28] Blair, M. F., "Boundary-Layer Transition in Accelerating Flow With Intense Freestream Turbulence: Part 1—Disturbances Upstream of Transition Onset," *J. Fluids Engineering*, **114**, 313-321 (1992).

[29] Volino, R.J., "A New Model for Free-Stream Turbulence Effects on Boundary Layers," *ASME Journal of Turbomachinery*, **120**, 613-620 (1998).